

Grid search modeling of receiver functions: Implications for crustal structure in the Middle East and North Africa

Eric Sandvol, Dogan Seber, Alexander Calvert, and Muawia Barazangi

Institute for the Study of the Continents, Cornell University, Ithaca, New York

Abstract. A grid search is used to estimate average crustal thickness and shear wave velocity structure beneath 12 three-component broadband seismic stations in the Middle East, North Africa, and nearby regions. The crustal thickness in these regions is found to vary from a minimum of 8.0 ± 1.5 km in East Africa (Afar) region to possibly a maximum of 64 ± 4.8 km in the lesser Caucasus. Stations located within the stable African platform indicate a crustal thickness of about 40 km. Teleseismic three-component waveform data produced by 165 earthquakes are used to create receiver function stacks for each station. Using a grid search, we have solved for the optimal and most simple shear velocity models beneath all 12 stations. Unlike other techniques (linearized least squares or forward modeling), the grid search methodology guarantees that we solve for the global minimum within our defined model parameter space. Using the grid search, we also qualitatively estimate the least number of layers required to model the observed receiver functions' major seismic phases (e.g., PS_{Moho}). A jackknife error estimation method is used to test the stability of our receiver function inversions for all 12 stations in the region that had recorded a sufficient number of high-quality broadband teleseismic waveforms. Five of the 12 estimates of crustal thicknesses are consistent with what is known of crustal structure from prior geophysical work. Furthermore, the remaining seven estimates of crustal structure are in regions for which previously there were few or no data about crustal thickness.

1. Introduction

In the Middle East and Africa there is only very sparse coverage of three-component broadband seismic stations (Figure 1). In order to improve knowledge of the crustal seismic velocity structure in the regions we have used receiver functions for all broadband stations located in the Middle East and North Africa. By inverting these receiver functions we place constraints on Moho depth and average shear wave velocities in regions where few geophysical measurements have been made. We have opted to determine first-order features of the crust and uppermost mantle; therefore we only interpreted the first 20 s of the teleseismic P wave coda.

Receiver function inversion, both quantitative and qualitative, has become a widely used seismological technique to obtain shear wave velocity structure beneath single, three-component seismic stations [e.g., *Phinney*, 1964; *Burdick and Langston*, 1977; *Langston*, 1979; *Owens et al.*, 1988]. The receiver function technique has the advantage of eliminating, given certain approximations, many of the complexities (source and instrument response) of a seismogram that complicate interpreting teleseismic body waves (Figure 2). Figure 2 shows the idealized case for receiver function interpretation. Fitting the PS_{Moho} phase in a receiver function has become a very common way to estimate crustal thickness and crustal S wave velocity, as this phase is generally observed globally. Furthermore, $PS_{Moho}S$ and $PP_{Moho}S$ phases, when observed, can be used to constrain Poisson's ratio [*Zandt and Ammon*, 1995]. More recently, the nonuniqueness and

the relative lack of stability of the receiver function inversion have also been well documented [e.g., *Ammon et al.*, 1990; *Sheehan et al.*, 1995; *Gurrola et al.*, 1996]. The nonuniqueness problem with receiver function interpretation is a result of having more unknowns than independent data (i.e., being under determined). Receiver functions are primarily sensitive to S wave velocities (V_s) but they are also a function of P wave velocity (V_p) and density. In order to reduce the number of unknowns we must assume (1) a Poisson's ratio (relating V_p to V_s), and (2) Birch's law (relating V_p to density). Using these assumptions, we can greatly reduce the number of model parameters in our inverse problem and make the problem less under determined. In order to address the lack of stability (i.e., initial model dependence) of receiver function waveform inversion methods, algorithms such as simulated annealing and the genetic algorithm have been employed [*Zhao and Frohlich*, 1996]. However, even with these techniques there is no guarantee that one will obtain the true global minimum due to the instability of the receiver function waveform inversion. Furthermore, *Zhao and Frohlich* [1996] attempted to find the minimum number of model parameters required to fit the teleseismic seismograms. Another approach used to resolve crustal structure using receiver functions has been to forward model waveforms [*Cassidy*, 1995; *Baker et al.*, 1996]. This method is especially useful when taking into account three- or two-dimensional structure or when trying to model complicated velocity gradients.

Methods have been designed to overcome this lack of stability by avoiding the deconvolution process and directly modeling the teleseismic P wave coda [*Zhao and Frohlich*, 1996]. This technique has the disadvantage of not completely accounting for source-side structure. We have used deconvolution in order to be able to stack our receiver functions, as is essential for bringing out coherent portions of the receiver function waveform. In order to

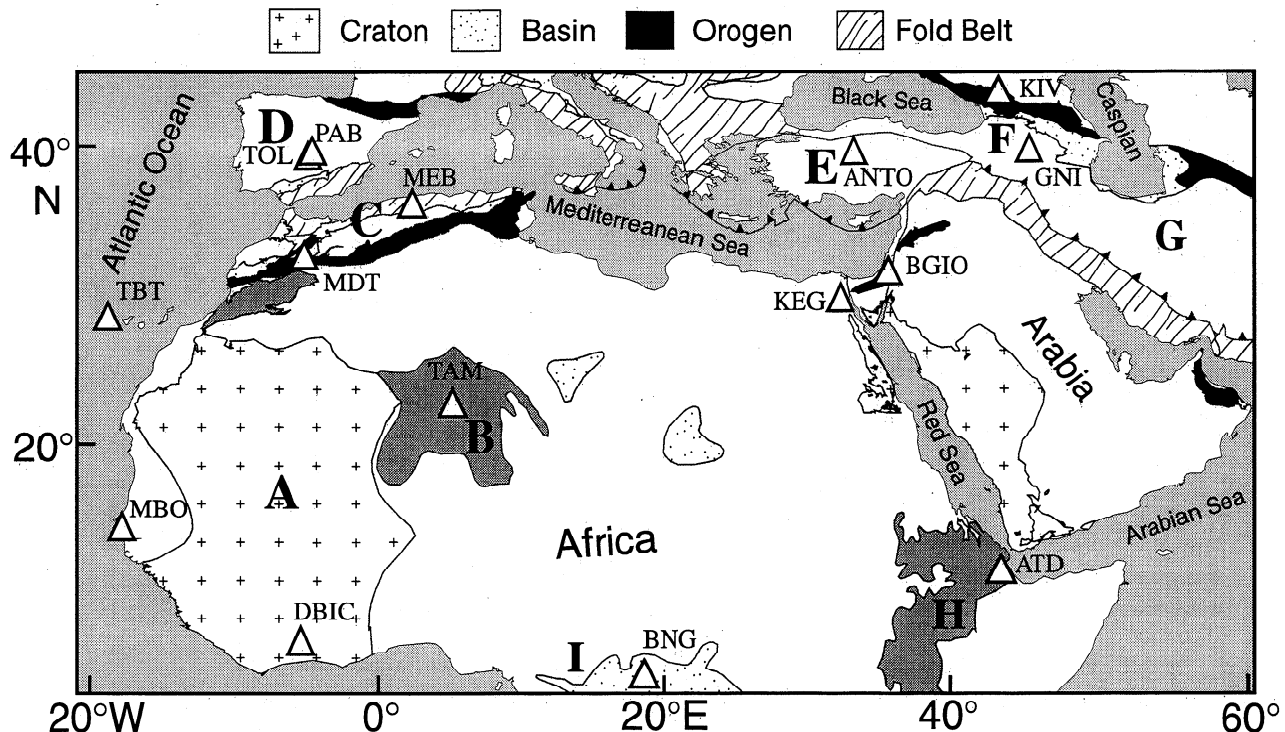


Figure 1. A simplified tectonic map of the Middle East and North, central, and western Africa. The tectonic units shown are primarily those in which we have a broadband station. Broadband stations are shown as open triangles. (A) West African Craton, (B) Hoggar hot spot, (C) Atlas mountain belt system including the High, Middle, and Tel Atlas Mountains, (D) Iberian Meseta, (E) Anatolian block, (F) Anatolian Plateau, Lesser Caucasus, and Greater Caucasus (shown as solid areas), (G) Iranian Plateau, (H) East African Rift System, and (I) Congo Basin and craton.

account for local minima, we used a grid search technique which guarantees that only the global minimum will be found for a given parameterization. Furthermore, in order to estimate how robust this minimum is, we applied a jackknife resampling scheme to estimate a confidence region for each of the model parameters.

1.1. Brief Summary of Previous Geophysical Studies

The Middle East and North Africa are excellent regions in which to employ a grid search technique to estimate crustal structure and thickness because there have been only a few regional-scale geophysical observations. Furthermore, we will be able to test this technique on very diverse crustal structure and in very different tectonic environments. Combining the grid search with our stability test, we were able to make estimates of crustal structure along with quantitative estimates of the resolution of the inversion. In the Middle East, there have been a number of refraction studies that provided estimates of basement and crustal thicknesses [e.g., *Ginzburg and Folkman*, 1980; *Ginzburg et al.*, 1981; *Yuval and Rotstein*, 1987; *El-Isa et al.*, 1987]. Both gravity and refraction profiles have constrained the crustal structure in Israel, although we have found some disagreement among various refraction velocity models in the region. Moho depths range from 28 to 34 km near station BGIO (Bar Giyyora, Israel) and from 8 to 11 km beneath Djibouti [*Laughton and Tramontini*, 1969; *Makris and Ginzburg*, 1987]. We are able to test the grid search technique by comparing our model and error estimates with these independent measurements of crustal structure. However, in North Africa the number of regional-scale geophysical measurements is very limited. In Egypt and Morocco, there have

been a few measurements of crustal thickness from refraction experiments [*Makris et al.*, 1988; *Wigger et al.*, 1992] that can be compared to our results. In central Spain, there have been a number of refraction and Deep Seismic Sounding (DSS) profiles which found the crust to be 32 [*Surinach and Vegas*, 1988] and 34 km thick [*ILHA DSS Group*, 1993] in central Spain as well as receiver function studies which estimated the crustal thickness to be 29 km [*Paulssen and Visser*, 1993].

1.2. Tectonic Setting

There are numerous and diverse tectonic regimes in the Middle East and Africa (Figure 1); hence it is critical to our understanding of these regions to have some knowledge of crustal thickness. In the Middle East the Dead Sea fault system is thought to be a transtensional feature associated with regional crustal thinning. Continental collision is taking place along the Bitlis suture, which has led to the subsequent escape of the Anatolian block and the uplift of the Iranian-Anatolian Plateau. Because little is known about the crustal structure in this region, even single station models are important. In Africa the tectonic setting is dominated by the African craton. However, there is a large intracontinental zone of deformation in the Atlas system in North Africa. The question of whether or not a crustal root exists in this intracontinental mountain belt is critical to determining the compensation mechanism for the Atlas system.

2. Grid Search Modeling of Receiver Functions

In order to solve the receiver function inverse problem given its lack of stability and nonuniqueness, we have employed a grid

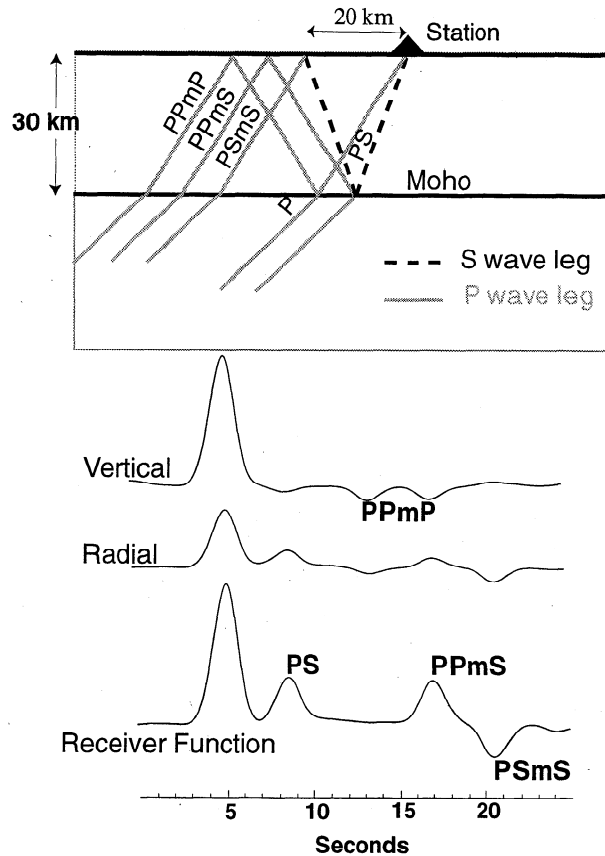


Figure 2. A schematic ray-tracing diagram for a hypothetical P wave incident on a 30 km thick crust. The light gray rays correspond to a P wave leg, while the dashed rays are S waves. The radial and vertical component synthetics were created with the reflectivity synthetic seismogram algorithm. Note that the PS Moho ray path is generated at the Moho roughly $10 \text{ to } 15 \text{ km} (\text{crustal thickness} * \sin(\text{incidence angle}))$ from the station.

search scheme with which we are able to easily incorporate a priori constraints and guarantee a complete search throughout the parameter space, while also avoiding the use of any initial models. The advantage of a grid search scheme is the guarantee that within the limitations of our grid spacing and parameterization, we will solve only for the global minimum. Furthermore, our approach will attempt to achieve the minimum length (i.e., simplest) velocity model at the expense of fitting our observed waveforms exactly. When trying to solve the receiver function inverse problem, one must reduce the number of model parameters to a number which is roughly equivalent to the number of observations (roughly speaking the observations are travel times and amplitudes of phases in the receiver function waveform). We have used the standard assumption of Birch's law and a Poisson's ratio of 0.25, although in certain cases we solved for a bulk crustal Poisson ratio. These assumptions reduce the number of model parameters to layer thickness and S wave velocity for each layer as well as a half-space velocity.

2.1. Grid Search Method

In order to invert the observed receiver function stacks for the crustal shear wave velocity structure, we apply a two-step grid search method combined with a jackknife error estimation technique (Figure 3). A reflectivity synthetic seismogram algorithm, initially developed by *Kennett* [1984] and used in

many subsequent receiver function studies [e.g., *Ammon et al.*, 1990], is used to create our synthetic receiver functions. To invert the receiver function data reliably for crustal and uppermost mantle shear wave velocity structure, we employed a grid search scheme using a maximum of six layers in our model. It should be noted here that the half-space (mantle shear wave velocity) is in practice unconstrained by the receiver function waveforms; furthermore, we have found that the our grid search results are generally insensitive to the half-space velocity. We have chosen a maximum of six layers since it is unlikely that we will be able to uniquely resolve a higher number of layers because of the number of phases that can usually be identified within a receiver function waveform. Using an assumed maximum and minimum possible thickness and shear wave velocity for each layer, the least squares difference between the observed and synthetic receiver functions is minimized. We determined these maximum and minimum values for each of the model parameters through a combination of a priori knowledge of the crustal structure in the region and trial and error. If a grid search solution contained model parameters at or near the edge of the grid

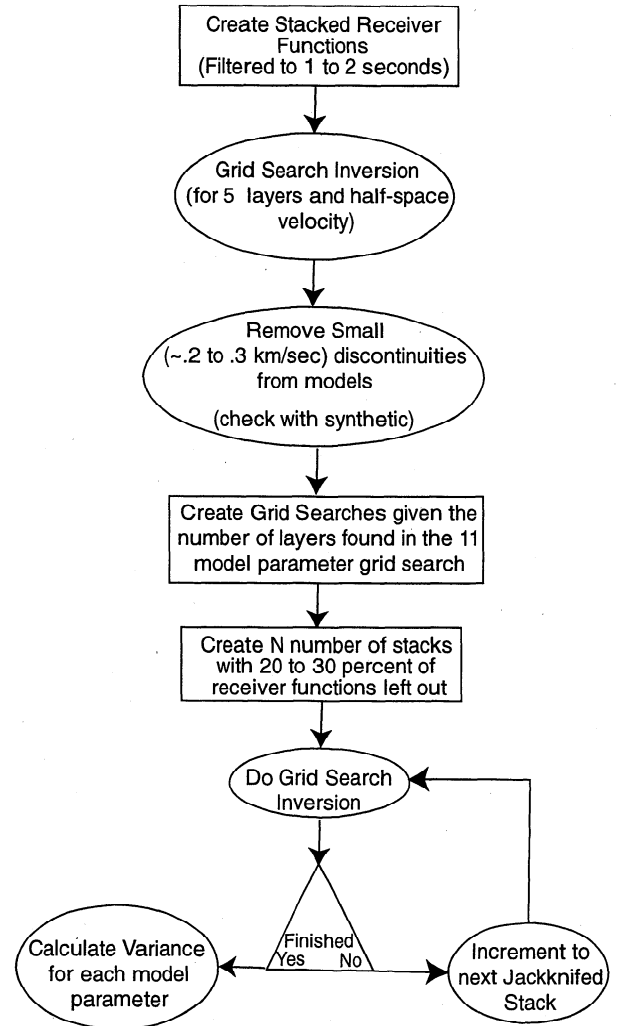


Figure 3. Flowchart showing the generalized procedure used in inverting and estimating the errors associated with each of the optimal shear wave velocity models. This approach is a systematic and generalized method to infer first-order crustal structure from teleseismic P wave coda.

Table 1. Minimum and Maximum Values and the Grid Spacing for Each Model Parameter Used in Each Station's Grid Search Receiver Function Inversion

Layer	ΔV_s , km/s	ΔD , km	Min V_s , km/s	Max V_s , km/s	Min D , km	Max D , km
<i>Station ANTO</i>						
1	0.1	2	2.70	3.50	7	13
2	0.1	2	3.04	3.84	14	22
3	0.1	2	3.14	3.84	4	10
4	0.1	2	3.54	4.24	1	5
5	0.1	1	4.54	4.64	5	5
<i>Station ATD</i>						
1	0.1	1	2.80	3.70	1	6
2	0.1	2	3.00	3.60	2	8
3	0.1	2	3.20	3.90	2	8
4	0.1	2	3.44	4.34	2	8
5	0.1	1	4.34	4.64	5	5
<i>Station BGIO</i>						
1	0.1	2	2.74	3.44	1	7
2	0.1	2	3.24	4.04	8	18
3	0.1	2	3.34	4.24	8	20
4	0.1	2	4.04	4.54	14	20
5	0.1	2	4.54	4.64	5	5
<i>Station BNG^a</i>						
1	0.1	1	2.90	4.50	28	55
2	0.1	2	4.34	4.74	2	8
3	0.1	2	4.64	4.84	4	4
4	0.1	2	4.64	4.84	4	4
<i>Station DBIC^a</i>						
1	0.1	1	3.50	4.20	20	50
2	0.1	1	3.54	4.24	1	7
3	0.1	1	4.64	4.84	1	7
4	0.1	1	4.64	4.84	5	5
<i>Station GNI</i>						
1	0.1	2	3.04	3.94	26	46
2	0.1	2	3.34	4.24	6	12
3	0.1	2	3.84	4.44	2	10
4	0.1	2	3.94	4.54	12	20
5	0.1	1	4.54	4.74	5	5
6	0.1	1	4.64	4.74	5	5
<i>Station KEG</i>						
1	0.1	2	2.90	3.30	2	8
2	0.1	2	3.40	4.05	4	12
3	0.1	2	3.40	4.15	10	22
4	0.1	2	3.74	4.44	6	14
5	0.1	1	4.54	4.74	5	5
<i>Station KIV</i>						
1	0.2	2	3.30	4.14	6	14
2	0.2	2	2.84	3.74	4	10
3	0.2	2	2.84	3.84	4	12
4	0.2	2	3.64	4.44	16	30
5	0.2	1	4.54	4.74	5	5
<i>Station MDT</i>						
1	0.1	2	3.70	3.90	2	8
2	0.1	2	3.30	3.90	4	8
3	0.1	2	3.44	4.34	10	16
4	0.1	2	3.64	4.44	6	22
5	0.1	1	4.44	4.74	4	4
6	0.1	1	4.64	4.74	4	4
<i>Station PAB</i>						
1	0.1	2	3.10	3.80	4	12
2	0.1	2	3.20	3.90	4	10
3	0.1	2	3.44	4.34	4	10
4	0.1	2	3.74	4.54	4	10
5	0.1	1	4.34	4.84	5	5
<i>Station TAM</i>						
1	0.1	1	2.80	3.30	1	5
2	0.1	2	3.00	3.90	8	18
3	0.1	2	3.20	4.10	8	20
4	0.1	2	3.44	4.44	4	14
5	0.1	1	4.54	4.74	5	5

Table 1. (continued)

Layer	ΔV_s , km/s	ΔD , km	Min V_s , km/s	Max V_s , km/s	Min D , km	Max D , km
<i>Station TOL</i>						
1	0.1	2	3.10	3.80	4	12
2	0.1	2	3.20	3.90	4	10
3	0.1	2	3.44	4.34	4	10
4	0.1	2	3.74	4.54	4	10
5	0.1	1	4.34	4.84	5	5

V_s and D represent shear velocity and layer thickness, respectively.
^aPoisson's ratio grid search interval is 0.01 between 0.22 to 0.30.

boundaries, then another maximum or minimum was tried. We were also able to use a priori knowledge from past geophysical results to set our grid search boundaries.

The grid spacing for the shear wave velocity is 0.1 km/s and 2 km for layer thickness and in some cases 1 km for the first layer (basement thickness, see Table 1). This parameterization corresponds to a much finer grid search of the velocity space than with thickness space. This tends to make velocity appear more sensitive to noise than to layer thickness (Figure 4). This can be demonstrated with the slope of the depth-velocity trade-off: for shallow discontinuities this slope is more sensitive to the velocity than the layer thickness.

In order to further reduce the computation time of the grid search inversion, we decimated the stacked receiver functions down to five samples per second. Since the receiver functions are filtered to 1.5 Hz and below, this did not cause any aliasing problems or differences in bandwidth between the synthetics and the observed receiver functions. This decimation, along with several other minor optimizations to the synthetic receiver function generator, enabled the calculation of approximately 150 synthetics per second on a SPARC Ultra 2 workstation.

Only 9 to 11 model parameters are used in the inversion (four to five layers for which the layer thickness, shear wave velocity, and a half-space velocity are modeled), so the receiver function inversion's nonuniqueness problem is further reduced compared to a 20-layer parameterization. The longer-period receiver functions are fit reasonably well by a five-layer model. A Poisson's ratio grid search spacing of 0.01 with a maximum and minimum of 0.30 and 0.22, respectively, was used to two stations located on the African shield. The sensitivity of receiver functions to Poisson's ratio, when Moho multiples are present, has been well established [e.g., Zandt and Ammon, 1995]. We have found an optimal bulk Poisson's ratio of 0.25 for these two stations. For the other 10 stations, we found that either (1) we were able to fit the observed waveforms, including multiples when present, without varying Poisson's ratio or (2) the complex receiver functions required a five- or six-layer parameterization.

The grid search scheme allows us to map the RMS error surface (Figure 4). This allows us to examine, qualitatively, the error surface for multiple or local minima (i.e., to test for nonuniqueness). Figure 4 is a portion of the nine-dimensional error surface derived from our grid search inversion method, in which we do not see evidence of large local minima that are located far from the global minima. The progressive broadening of the minima with increasing layer depth is an indication that errors are propagating from the upper layers to the lower one. However, this is only a portion of the error surface from the grid search inversion. The difficulty in using the error surface in determining a confidence region is the need to quantitatively

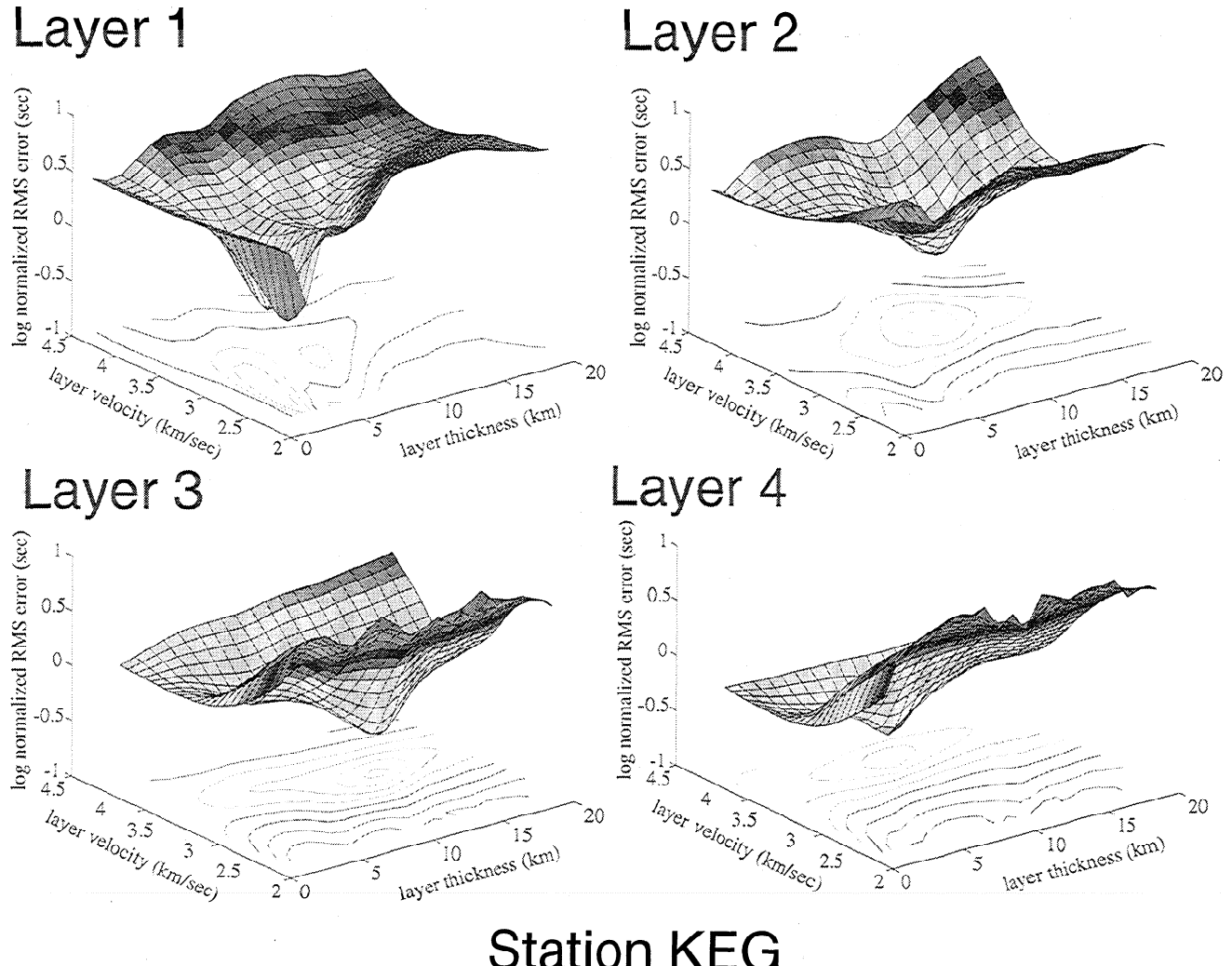


Figure 4. Plots showing an example of RMS error surfaces for the stacked receiver function from station KEG. The layer error surfaces were obtained by holding the other eight model parameters constant, at the final model, while the layer shear wave velocity and thickness were allowed to vary. Note that in layer one the minimum's slope is biased toward the velocity axis; this is a result of a finer grid spacing for the velocity than the thickness model parameter.

estimate the correlated noise contained within the receiver function time series [e.g. Sandvol and Hearn, 1994]. This becomes a difficult problem because neither the tangential receiver function nor the noise preceding the deconvolved radial and vertical seismograms provide a reasonable estimate of the correlated noise time series. Therefore we have avoided using the error surface to estimate our confidence limits.

We have found that comparisons between the grid search technique and the linearized least squares (LLS) method yield different results. For those receiver functions that are relatively simple in nature (i.e., only a PS_{Moho} phase), the results are similar given a starting model that is close to the final solution. We have employed Ammon *et al.* [1990] method of using multiple starting models in order to make our comparison. We found significant differences for many of the resulting models obtained for stations KEG and BGIO (Figure 5). The mean of the LLS models for station KEG agreed with our grid search results; however, the results from the LLS inversions for station BGIO tended to be biased toward a thicker crust than that of our grid search results. It should be noted that many of the LLS for station BGIO solutions did agree with our grid search model; however, five of

the models yielded crustal thicknesses of more than 35 km. We have also found that the smoothing constraint often used with the LLS inversions can potentially cause significantly different velocity models, as seen in the final models for station BGIO. We did try a number of different smoothing parameters and LLS model perturbations in order to test when the LLS method diverged from the grid search solution. We found significant differences between the grid search solution and the LLS solution for all solutions which did not have initial models near the solution. Inversion techniques, such as simulated annealing and genetic algorithms, should improve this performance.

2.2. Resolution and Error Analysis

After obtaining the results from our grid search, we qualitatively analyzed, for each station's best model, each layer as to whether or not the layer contributed a significant amount of energy to the synthetic. We have performed this exercise for all 12 stations. Stations BNG and DBIC were initially modeled using a four-layer crust, but we found that the grid search procedure effectively chose a one-layer crust; therefore we could

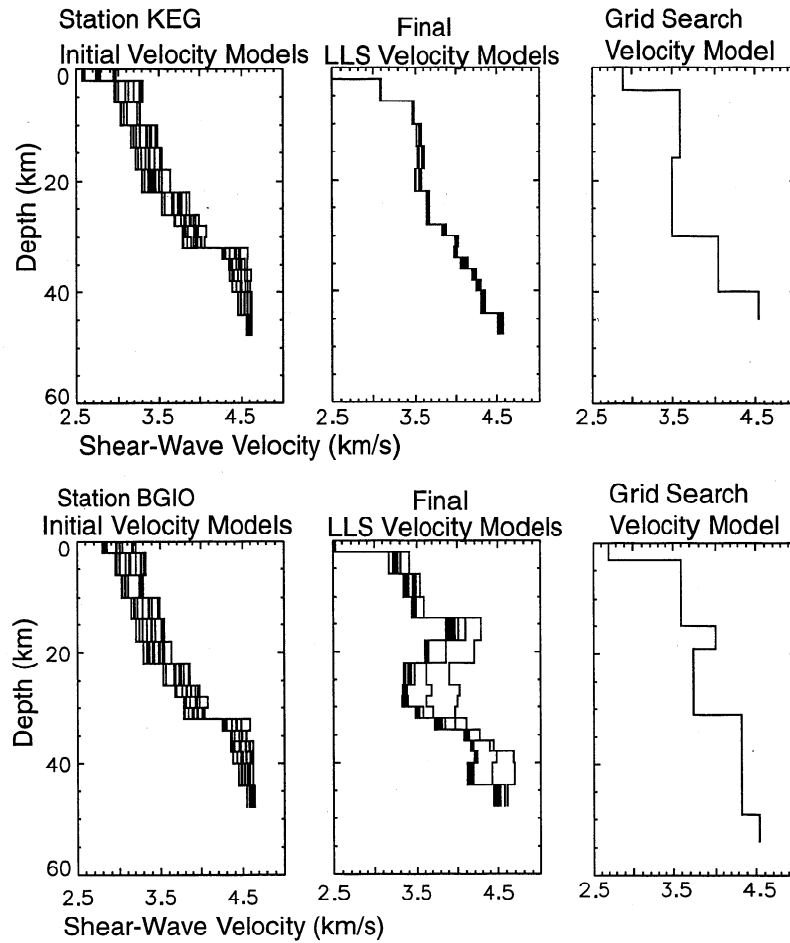


Figure 5. A comparison of the linearized least squares (LLS) and grid search inversions for two stations, KEG and BGIO, in the Middle East (see Figure 1). We have used a smoothing parameter of 0.1 and a damping parameter of 0.01 for the LLS inversion. We have also used Ammon *et al.*'s [1990] method of using an initial velocity model suite in order to measure the nonuniqueness of the inversion. The LLS inversion also utilized 25 layers with fixed layer thicknesses of 2 km. Our grid search inversion used a five-layer over half-space model. Note that the differences between station KEG's grid search and LLS final model(s) can be attributed to the smoothing constraint used. Station BGIO's grid search final model is considerably different from many of the final models obtained from the LLS technique.

effectively model the crust with only two parameters (i.e., shear velocity and thickness). Synthetic receiver functions fit data recorded by station BGIO significantly better by including more than four layers in the grid search because of the complexity of the BGIO receiver function. Owing to computational limitations with our jackknife error estimation technique, we used the best fit for four layers beneath BGIO (Figure 6), however we do show the results of a five layer grid search result without error estimates (Figure 6). The limitation of the number of model parameters has allowed us also to employ either a bootstrap or a jackknife resampling error estimation scheme, and we will see later in the results that the resolution at this station is such that it is unlikely that we can resolve a multilayer velocity model.

When estimating errors of our inversion results, we normally require an estimate of the noise contained within the receiver function stacks. Estimating an accurate and robust "noise time series" from the receiver function data is usually not possible [Paulssen and Visser, 1993]. The difficulty in estimating the true noise contained within the stacked receiver functions has led us to avoid constructing confidence regions from the error surface. Bootstrap error estimations for receiver function inversions via an estimated noise time series or randomized residuals are

problematic because the definition of a correlated residual time series is not obvious.

A jackknife data resampling technique has the advantage of not requiring the estimation of a noise vector or time series, and these techniques have been proven to yield unbiased and robust error estimates for both linear and nonlinear inversions [Efron, 1982; Wu, 1986; Tichelaar and Ruff, 1989]. Therefore we have chosen this resampling method to estimate the stability and errors of our shear wave velocity model estimations. An example of this method applied to the receiver function inversion for station KEG is shown in Figure 7. The drawback of this technique is that it will not account for systematic errors in the data. Recently, Gurrola *et al.* [1996] have suggested that such systematic errors exist within receiver function waveforms. This would then lead to systematic offsets in the estimated velocity models that would not be accounted for in either a bootstrap or jackknife resampling method. We tested for effects of such systematic errors for stations where Moho depths have been measured using other geophysical techniques.

Wu [1986] derived an expression for the formal error utilizing a jackknife resampling scheme. We can write, after Wu [1986], the expression for the formal error:

$$\sigma_{\text{jackknife}}^2 = \frac{k - p + 1}{n - k} \sum_{i=1}^N (\omega_i - \bar{\omega})^2 \quad (1)$$

where k is the total number of degrees of freedom (DOF) contained within the jackknife waveform stack, p is the number of model parameters (2 times the number of layers plus one), n is the total DOF summed over each of the receiver functions contained within the stack, N is the total number of model parameters, ω_i is

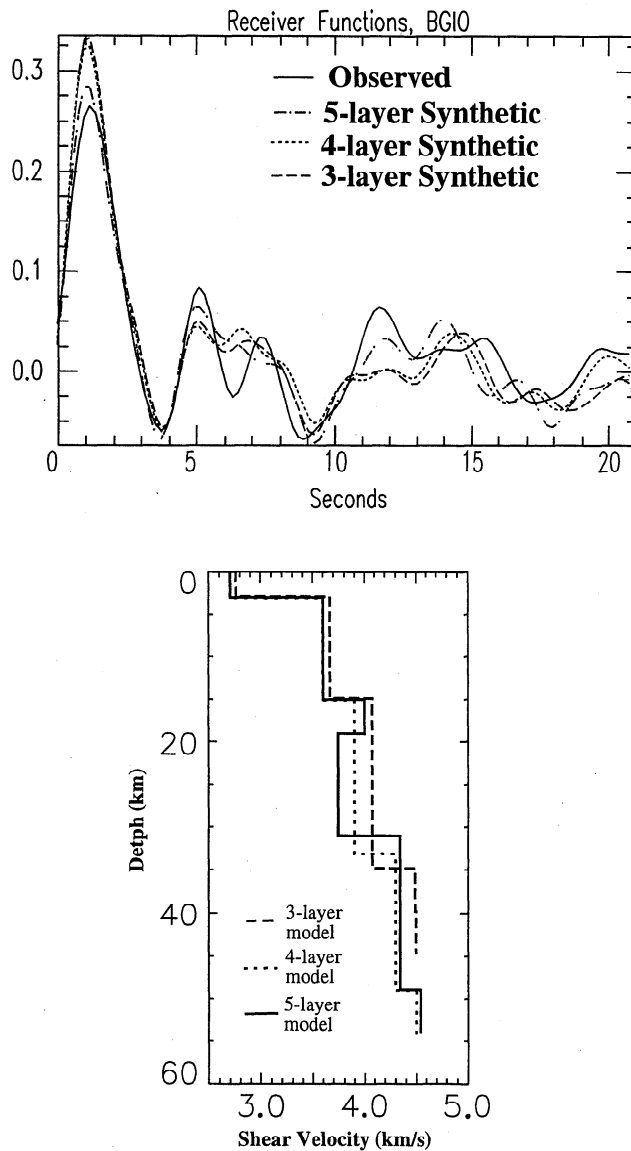


Figure 6. A comparison of four- and five-layer grid search solutions for station BGIO. (top) The synthetic waveforms corresponding to a shear velocity model obtained from a grid search using 11 model parameters (five-layer crust over a mantle half-space), using a 9 model parameter grid search inversion (four-layer crust over a mantle half-space), and the observed stacked receiver function. (bottom) The velocity models obtained from both inversion schemes. Teleseismic waveforms from station BGIO are the most complex of the 15 stations that we examined; hence we had the most difficulty modeling the BGIO receiver functions with a four-layer model. Station BGIO is the only station where we observed a significantly better fit, between the observed and computed waveforms, for a five-layer model than a four-layer model.

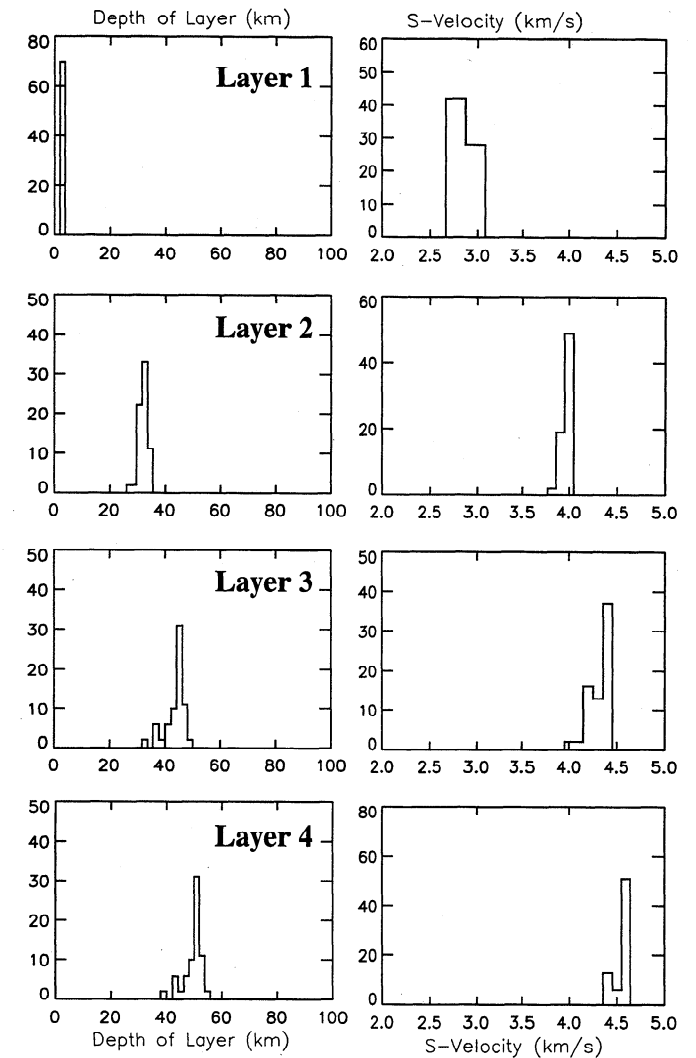


Figure 7. A set of histograms corresponding to eight model parameters used in the KEG station grid search inversion. We have obtained these histograms by inverting 121 jackknife receiver function stacks. We used a delete-3 jackknife resampling scheme to produce these receiver function stacks. The large variance in the model parameters indicates either a strong azimuthal variation in the data or a relatively unstable inversion result (i.e., large variance in the data). We have examined the data for evidence of azimuthal effects and have found little evidence given our data set.

the estimated model parameter for each jackknife resampled waveform data set, and $\bar{\omega}$ is the mean of the given model parameter (thickness or shear velocity for a given layer). We have estimated the DOF contained within each receiver function using the method of *Silver and Chan* [1991] and *Jenkins and Watts* [1968]:

$$\text{DOF} \approx 2\left(\frac{2E^2}{E_4} - 1\right) \quad (2)$$

where

$$E \approx \sum_{j=1}^{N-1} |u_j|^2 + 1/2(|u_0|^2 + |u_N|^2) \quad (3)$$

$$E_4 = \sum_{j=1}^{N-1} |u^4(j)| + 1/3(|u_0|^4 + |u_N|^4) \quad (4)$$

where $u(j)$ is the digital spectrum (i.e., Fourier transform of the receiver function waveform) with a frequency spacing of $1/T$, where T is the sampling rate; u_0 is the DC shift of the digital spectra. This approximation works well for this case since equation (1) is not very sensitive to the number of DOF because we are taking the ratio of the deleted DOF.

This technique gives an estimate of the receiver function stability, as long as there is a sufficient number of receiver functions that can create a "large" (≥ 50) number of resampled stacks. Note that equation (1) reduces to the calculation of the standard variance for the case where we delete all but one of our data vectors from our stacks. In order to test the robustness of this error estimator we tried a number of different re-sampling schemes (i.e., delete-1, delete-2, delete $n-1$, etc.) and compared the resulting error estimates. We found that the estimated errors for different resampling schemes varied by 20%. If k is nearly as large as n and thereby causing the normalizing term to be very large, the error estimator is biased upward.

3. Crustal Structure in the Middle East and North Africa

3.1. Data

We have collected over 1200 three-component seismograms, for the years 1988 through 1995, produced by 15 Federation of Digital Seismic Networks (FDSN), Global Seismographic Network (GSN), Mediterranean Network (MEDNET), Geoscope (French Global Seismographic Network), and GEOFON (German Global Seismographic Network) permanent broadband stations in the Middle East and North Africa (Figures 1 and 8a). These data were then reduced to 165 three-component seismograms which produced receiver functions with high signal to noise ratios. We have used waveforms from events located at distances between 35° and 85° in order to avoid problems with regional and core phases. We have examined all available records and eliminated those with signal to noise ratios of less than ~ 4 to 1, where we define noise as the seismic energy preceding the direct P arrival after deconvolution.¹

Our data selection is not restricted to deep earthquakes. P wave teleseisms with relatively simple vertical responses, whether from deep or shallow earthquakes, have been selected. Simple vertical component P wave waveforms should correspond to simple source-time functions. Receiver functions from small shallow events, taken from seismograms with simple first motions, showed strong coherence with receiver function waveforms from deep events. Receiver function stacks, shown in Figure 8, were created for data originating from several azimuths in order to attempt to obtain the average, with respect to azimuth, shear wave velocity model (Figure 9). We have stacked for only one distance ($\pm 10^\circ$) for mean distances of greater than 60° in order to avoid problems caused by move-out of the PS phases from differences in angles of incidence (i.e., differences in the ray parameter) [Cassidy, 1992].

We have attempted to eliminate the effects of large-scale lateral velocity heterogeneity by calculating the radial direction using the first half to three quarter wavelength of three-component teleseismic first motion. We have minimized the tangential component energy and then rotated the horizontal components into this corrected radial and tangential directions. Although this procedure will not remove the effect of smaller-scale crustal and upper mantle velocity heterogeneity, we have found that it does remove the effect of teleseismic ray bending resulting from large-scale mantle heterogeneity and reduce the effects of misaligned horizontal seismometers.

We have employed the commonly used "water level" spectral division technique [e.g., Langston, 1977; Ammon et al., 1990] to calculate each of the receiver functions used in this study. In order to solve for receiver functions that are sensitive primarily to first-order features, we have used a Gaussian filter with an $\alpha = 1.5$. Station GNI contained a large amount of 1 Hz noise, so we used an even longer period low-pass (Gaussian) filter ($\alpha = 1.0$). The Gaussian filter produced fairly coherent receiver functions that contained data with frequencies of 0.5 Hz. This filter limits, to a certain degree, the resolution of the shape and slope of the discontinuities within our velocity models. However, we are primarily interested in the first-order depth to these discontinuities and hence are willing to lose resolution of crustal structure in order to minimize the effects of small-scale "non-one-dimensional" structures beneath the receivers. The stacked receiver functions were not normalized in order to use the P wave amplitude to further constrain the near surface S wave velocity [Ammon et al., 1990]. Seismic data from 15 stations have been used to calculate high-quality receiver function waveforms (Figures 8b, 8c, and 8d). We have chosen not to use three of the 15 stations (MBO, TBT, and MEB) shown in Figures 8b, 8c, and 8d because we were not able to model the waveforms with a reasonable 1-D Earth model.

3.2. Results and Interpretations

Our estimates of the crustal velocity structure from receiver function waveform modeling are shown in Figure 10. In general, stations with relatively simple waveforms (i.e., simple PS Moho and its corresponding multiples) yield the most well constrained results. However, complicated waveforms can also produce well-resolved models if tighter constraints can be placed on the shallow structure. We used results from the jackknife error estimation to confirm this idea. The variance that we have observed in our data can be mostly attributed to variations in the waveform amplitudes since we have found that the mean crustal S wave travel time tends to stay fairly constant for each of the jackknife S wave velocity models.

Crustal thickness in North and central Africa is found to be between 36 to 43 km (Figure 10), except for station ATD which is located on either exposed oceanic crust or very thin continental crust at the northern end of the East African Rift system [Makris and Ginzburg, 1987; Mohr, 1989] (Figure 10). We have found a Moho depth of 8.0 ± 1.5 km for station ATD. Our crustal shear wave velocity model is in agreement with the prior geophysical studies. Searle [1975] demonstrated that this region blocks Lg as well as having relatively low Pn velocities [Makris and Ginzburg, 1987]. Each of these observations is consistent with a thin and relatively slow crust and uppermost mantle. The ATD station S wave velocity model indicates that there is a velocity gradient in the crust starting at ~ 2.9 km/s and reaching 4.0 km/s at 8 km. Station ATD is deployed on weathered basalt; this layer of

¹Supporting Data are available on diskettes or via Anonymous FTP from kosmos.agu.org, directory APEND (Username = anonymous, Password = guest). Diskette may be ordered from American Geophysical Union, 2000 Florida Avenue, N.W., Washington, DC 20009 or by phone at 800-966-2481; \$15.00. Payment must accompany order.

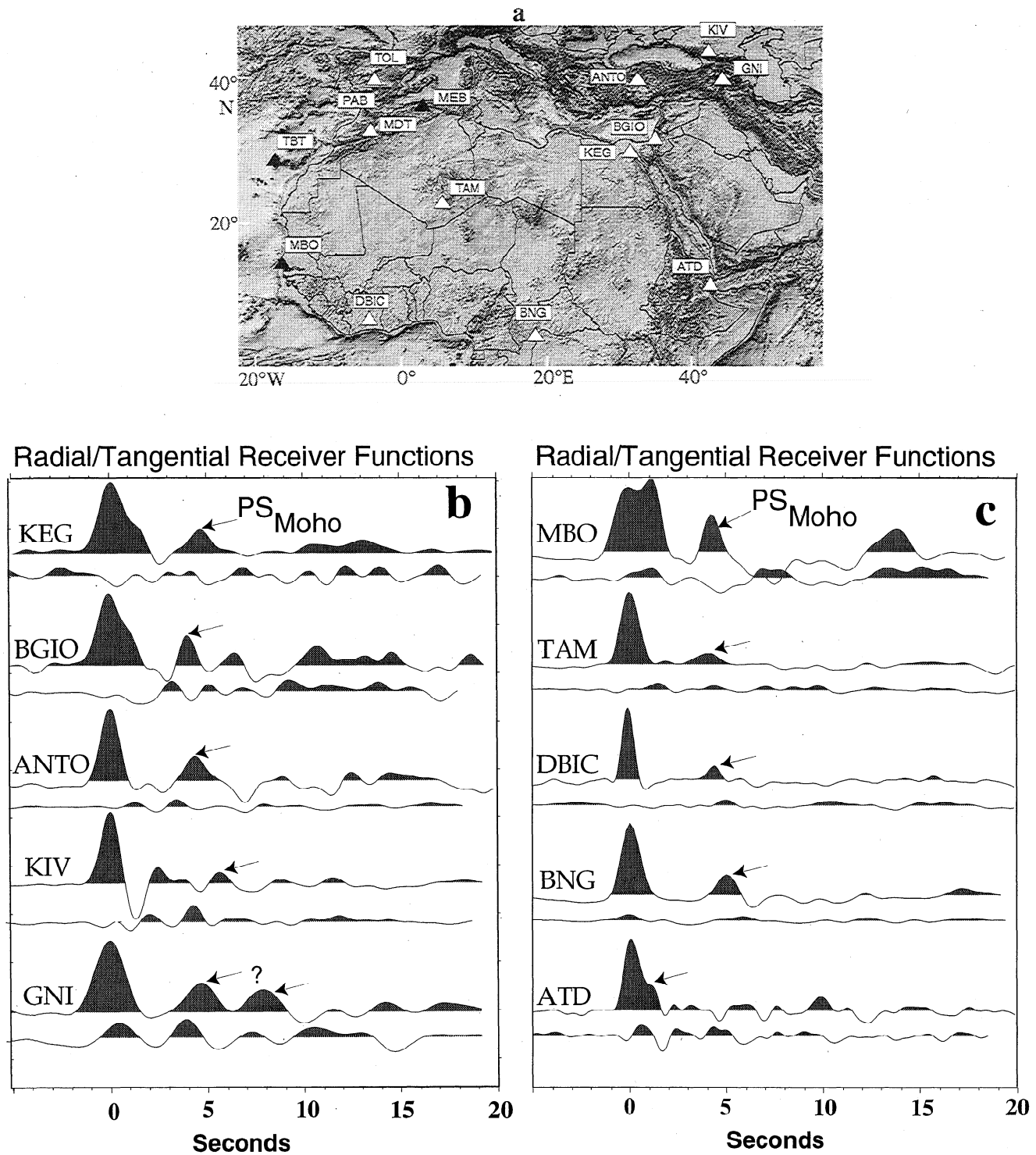


Figure 8. Map showing all stations for which a receiver function stack was computed. Only 12 of these stations (open triangles) were used to invert for a shear wave velocity model. The three that were not inverted were stations MBO, MEB, and TBT (solid triangles). All stacked radial and tangential receiver functions that have been computed for the Middle East and north, central, and western Africa are shown in Figures 8b, 8c, and 8d, respectively. Station names are shown on the left of the radial receiver function. The top trace, for each station, corresponds to the radial receiver function, while the bottom trace is the tangential receiver function. Several of these receiver functions were determined to contain waveforms that could not be modeled with a reasonable one-dimensional model and hence are not addressed in this paper. The extremely large PS_{basement} at the station MBO has made it very difficult to model with a one-dimensional velocity model. Stations TBT and MEB both had very noisy and incoherent waveforms.

Radial/Tangential Receiver Functions

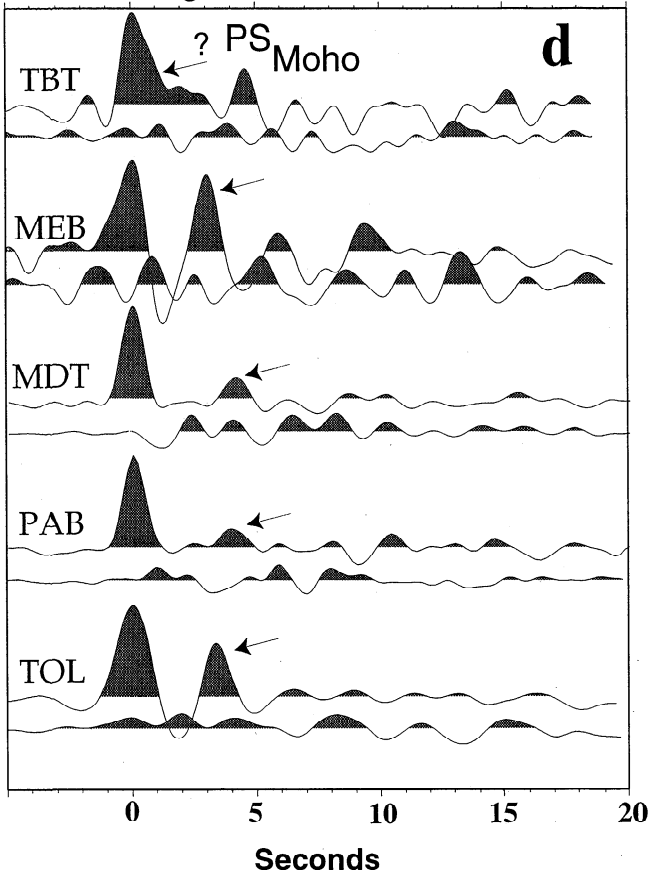


Figure 8. (continued)

weathered basalt explains the low surface velocities required to fit the P amplitude [Ammon et al., 1990].

In the stable African craton, there are three stations at which we have been able to estimate crustal structure. Station TAM, near the Hoggar hot spot, yields the most stable inversion results where 90 jackknife receiver function inversions all resulted in crustal thickness of 38 km (Figures 11 and 12). Figure 12 shows all of the jackknife velocity models that we have found for each station's S wave velocity models. This indicates that ignoring systematic errors, the variance of our estimate of crustal thickness is less than the one-half the thickness of the grid search spacing (1-2 km). This result is also an indication that the crustal structure surrounding station TAM is very homogenous. Similar crustal velocities and thicknesses were found for station DBIC; however, we have considerably less data to constrain this model. Consequently, our jackknife error estimates are not as reliable since we were not able to create more than 15 jackknife receiver function stacks. We did find little variance among these 15 jackknife models. It is not surprising that the most reliable data were discovered for broadband stations in the African craton (stations BNG and DBIC). This is a region where the one-dimensional Earth approximation is most valid. The Moho for station BNG, however, could not be modeled with one discontinuity due to the broadness of the PS_{Moho} phase. Our error estimates indicate that this is a robust measurement and that the crust to mantle transition is probably smooth rather than a sharp boundary (Figure 10b). Data from TBT and MEB in North and central Africa contain a large amount of noise in the computed

receiver functions. Station MBO contained a very large near-surface converted phase (Figure 8c) which would require an unrealistically shallow low-velocity anomaly. At all three of these stations (MBO, TBT, and MEB) it was impossible to model the observed receiver function waveforms with a suitable one-dimensional shear velocity model and hence we have not estimated crustal models for these stations. In the case of TBT and MEB the signal to noise ratio was very poor; however, at station MBO we had several high-quality receiver function waveforms. It is possible that focusing of a PS phase at the sediment-basement contact, caused by two- or three-dimensional velocity structure, is causing the large amplitude PS phases that we observe at this station.

For other stations in North Africa we have found that the crust is usually of the order of 40 km thick. Only near the Moroccan Atlas Mountains, at station MDT, do we find a crustal thickness less than 40 km. In North Africa we have obtained a crustal thickness of 36 km on the eastern edge of the Middle Atlas Mountains [Wigger et al., 1992] that also estimated a crustal thickness of 36 to 37 km beneath MDT. The absence of a significant root beneath the Middle Atlas system is probably a result of the fact that the mountain chain was initially a failed rift with a very thin crust which was subsequently inverted. The fact that there is no crustal root is probably an indication that the central Middle Atlas is overcompensated.

In Spain, there are two broadband stations within 50 km of one another (station TOL and PAB) which are both located within the Iberian Meseta. Inversion results from station PAB are fairly stable while results from TOL are very unstable (see Figures 11 and 12). The PAB and TOL optimal shear wave velocity models are relatively consistent; each having Moho depths of 34 km (see Table 2). Most other features in each of the two stations' velocity models are not consistent with one another; however, our error estimates indicate that these features cannot be reliably interpreted. Our poor waveform fits for station TOL also demonstrate that within our grid search upper and lower bounds, there is no one-dimensional velocity model which fits the observed receiver function waveforms (Figure 13). Our waveform fits for station PAB (Figure 13) are far superior to those for TOL, which is also consistent with our jackknife error estimates (Figure 10). The crustal thickness estimates are consistent with the interpretation of DSS profiles [ILHA DSS Group, 1993] which showed an average crustal thickness of 34 km near TOL and PAB, and refraction profiles [Surinach and Vegas, 1988] which showed an average crustal thicknesses of 32 km. Paulssen and Visser [1993] found a much thinner and faster crust (29 km) by inverting receiver functions derived from temporary stations in central Spain.

In Egypt, at station KEG, we have found a crustal thickness of 33 km. Makris et al. [1988] found crustal thicknesses of the order of 30 km (30 to 32 km) in northern Egypt, from refraction data that is consistent with our analysis at station KEG. At station BGIO our estimates seems thicker (33 km) than many of those from seismic refraction work. Yuval and Rotstein, [1987] give crustal thicknesses of 31 km near BGIO, and Ginzburg et al. [1981] estimated 29 to 30 km thick near BGIO. We may be seeing crustal thicknesses farther to the east, since all of the waveforms we have used are arriving from east-northeast, where the crust appears to thicken [Ginzburg and Folkman, 1980]. Basement depths from stations BGIO and KEG are also surprisingly consistent with prior geophysical/geologic

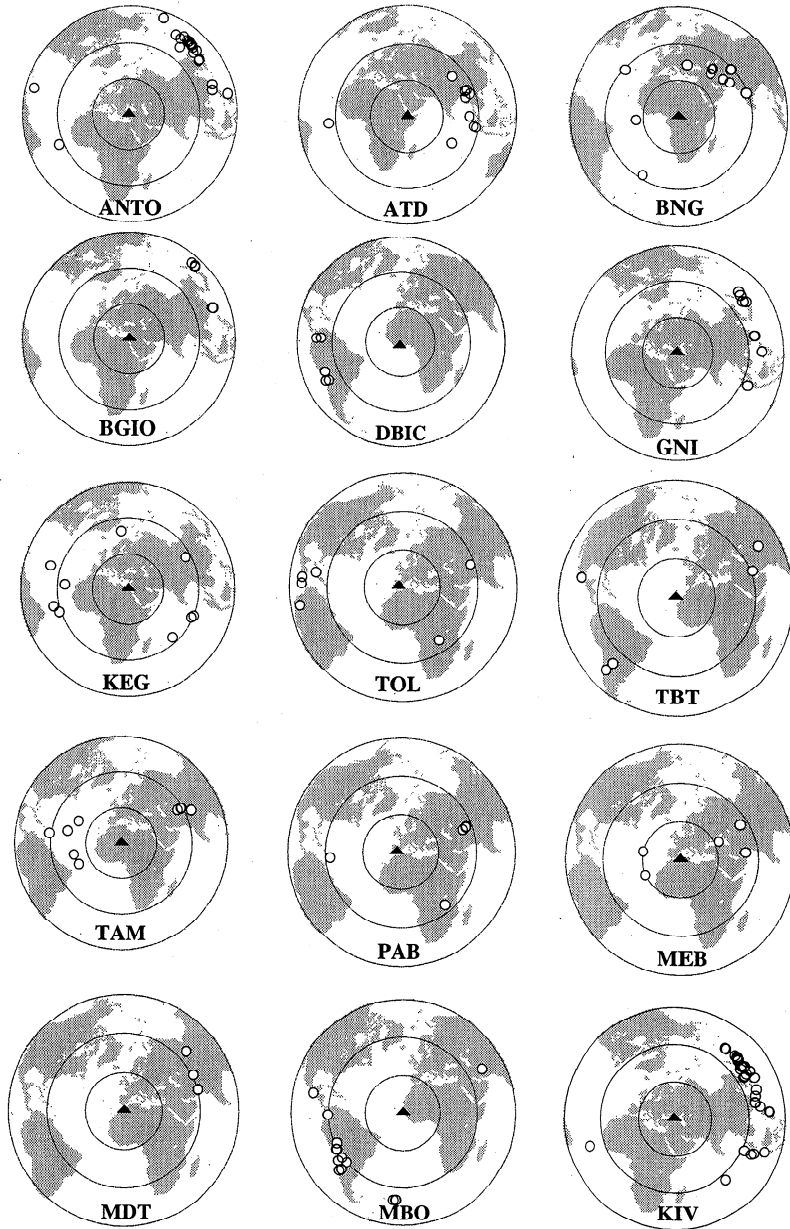


Figure 9. A plot of all events used in each stack for all 15 stations shown in Figure 8. The concentric circles represent 30° increments centered on each station shown. We have restricted our event to stations distances to between 35° and 85° but only stacked within $\pm 10^\circ$.

observations [Makris *et al.*, 1988; Hofstetter *et al.*, 1991]. Jackknife error analyses indicated that these two sediment thicknesses are robust measurements (Figure 10a). The error estimates for the sediment thicknesses are actually smaller than those for the depth to Moho errors. This is either a good indication that the errors are propagating from the shallow layers to the deeper layers or that the percent error in these models remains constant with depth.

We have also found evidence of a pronounced robust midcrustal low-velocity zone in the Greater Caucasus, beneath station KIV (Figure 10). First, we observe a very large amplitude, negative polarity PS phase, arriving 1.2 s after the P wave. There is very little azimuthal variation of the large negative PS phase, indicating that this low-velocity zone is not a small isolated pocket of slow material (roughly 40 km in diameter). Also, our

jackknife error estimates indicate this is a robust feature (Figures 11 and 12). This is the only low-velocity zone we have imaged, within our error estimates, out of the 12 stations we analyzed.

We observed two large, azimuthally coherent PS phases at station GNI in Armenia (Figure 8b). The first phase corresponds to a discontinuity at ~ 40 km, while the later phase corresponds to a 60-km discontinuity. Data at station GNI were observed to be of relatively low quality and to contain a large amount of noise within the stacked receiver function. The jackknife error estimates also indicated a relatively unstable solution (Figures 10 and 13); therefore which shear wave velocity discontinuity corresponded to the Moho was not clear. Given the high topography, one might expect to observe a crustal root in this region, so we have tentatively interpreted the second boundary to be the Moho discontinuity. Receiver functions also contained a

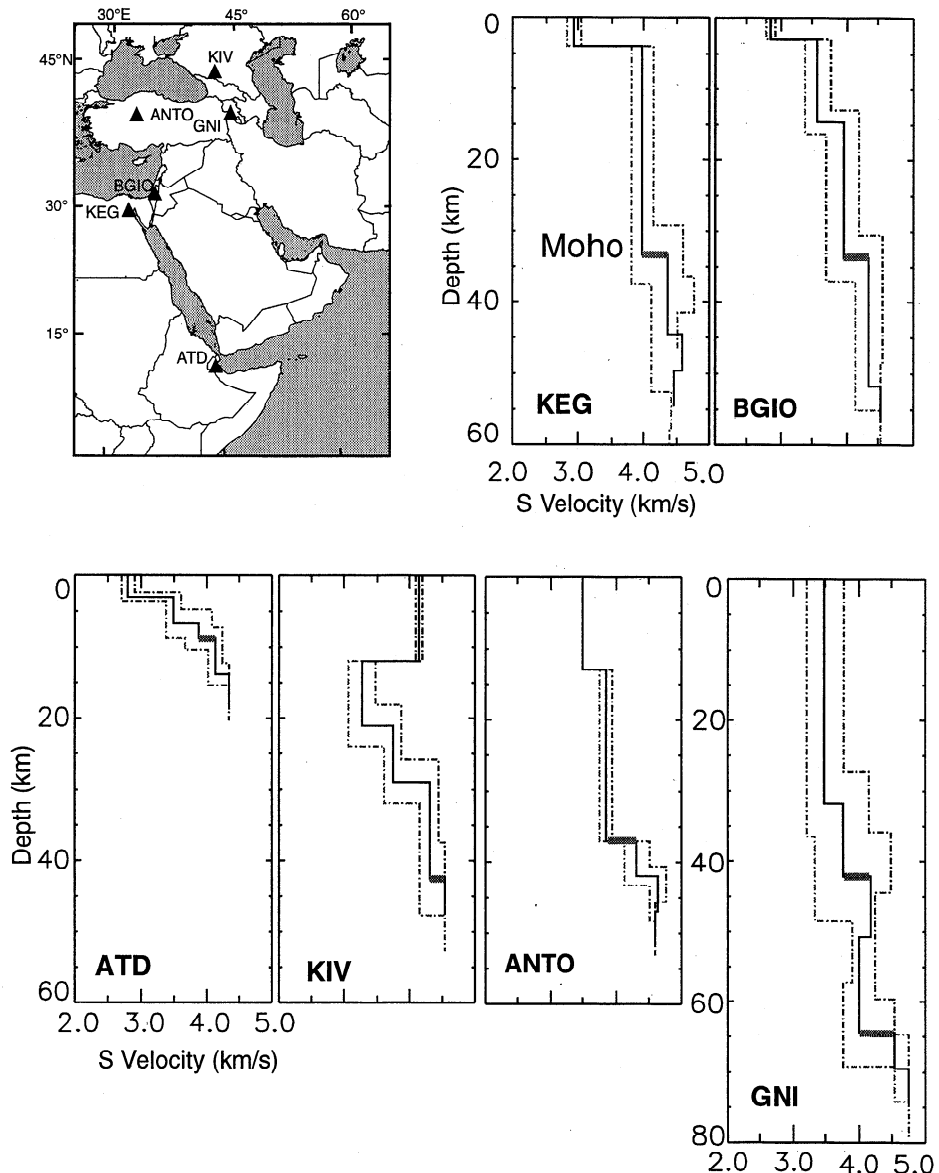


Figure 10a. Shcar wave crustal velocity models and the location of the interpreted Moho for six stations in the Middle East. Locations are shown of broadband stations in which sufficient data were available to compute a reasonably high quality stacked receiver function. Our interpreted Moho discontinuity is shown as a thick gray line on each model. The maximum and minimum models, obtained from the jackknife error estimations, are shown as dashed lines. Several models (e.g., models for stations KEG and BGIO) have larger velocity errors than layer thickness error estimates for shallow layers. This is a result of a coarser grid spacing for layer thickness than the velocity grid spacing. Also, the receiver function synthetics are also less sensitive to shear velocity than depth to the discontinuity for the shallow layers. This can also be seen in the gradient of the error surface near the minimum shown in Figure 4.

large amount of coherent and azimuthally dependent energy that appears on the tangential receiver functions. This may be an indication of a dipping Moho. It is also possible that crustal polarization anisotropy could be causing the PS_{Moho} phases to change polarization direction, thereby leading to the observed energy on the tangential component.

Within the center of the Anatolian block, analysis of receiver functions recorded at station ANTO yielded a relatively simple velocity model with a crustal thickness of 37 km. There have been very few reliable estimates of crustal thickness in this region; however, a crustal thickness of 37 km in this region is not unreasonable.

4. Discussion and Conclusions

Our study shows that grid search waveform modeling provides a robust and efficient method for determining depth to first-order crustal discontinuities. Using this method, we inverted stacked receiver functions for optimal and simplest shear wave velocity models as well as corresponding error estimates in the Middle East and North Africa (Figure 14) where no prior results exist. The method presented here has several advantages over prior receiver function techniques: (1) The grid search inversion has no dependence on an initial model, (2) the grid search inversion guarantees that we will solve for the global minimum within the

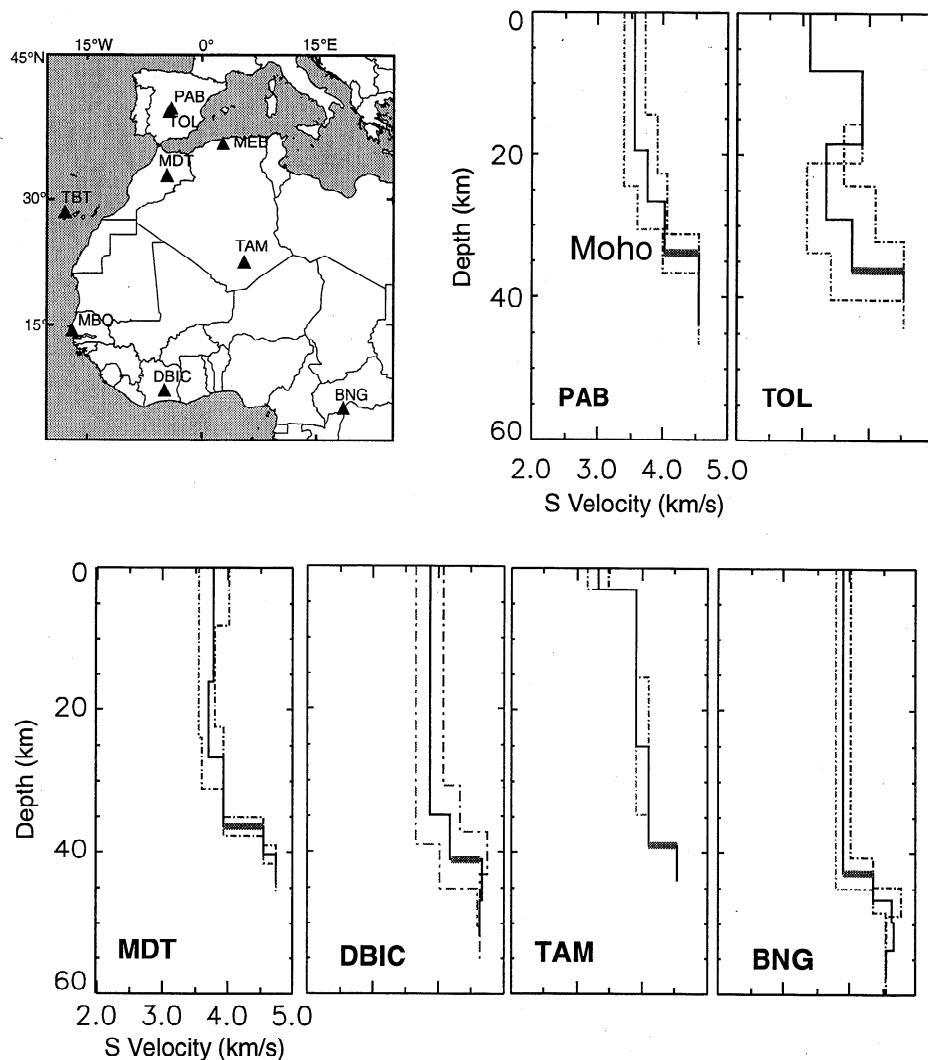


Figure 10b. Same as Figure 10a, except for Africa.

chosen parameter limits, (3) the jackknife error estimation gives a measure of the stability of the inversion, and (4) these methods allow for constraints from other independent studies (e.g., on shear wave velocity or depth to a discontinuity) to further strengthen the robustness of our results. The crustal thickness measurements we have made using these methods provide important constraints for future studies of seismic velocity structure and the geodynamic and tectonic processes taking place in the Middle East and Africa.

In western and central Africa we have found that the crust is consistently about 40 km thick. We have found slightly thicker crust at station BNG, in central Africa. We have also determined that the crust is fairly thick (~40 km) very close to the African coast at station DBIC. Station ATD, located in the Afar region of eastern Africa, is the exception to these observations. Velocity models for this station indicate that Djibouti is situated on either oceanic or very stretched continental crust. This is consistent with previous tectonic and geologic observations in the Afar [e.g., Mohr, 1989].

In the northern portion of the Middle East, our velocity models vary widely from very thick crust to approximately the global average crustal thickness. In the Lesser Caucasus beneath station GNI, we have found ambiguous evidence for a large crustal root,

although we have also observed another possible Moho discontinuity at 43 km depth (Figure 10a). In the Greater Caucasus, near station KIV, there is a relatively young volcano, the last eruption having occurred 2.8 Ma [Gazis et al., 1995], and associated calc-alkaline lava [Zonenshain et al., 1990]. This may imply the existence of a partially molten or highly heated midcrustal pluton related to recent subduction in the Greater Caucasus. The existence of a high heat flow anomaly in the Greater Caucasus [Cermak and Rybach, 1987] and the very large velocity contrast at this boundary (Figure 10a) are consistent with the existence of a magma chamber. Alternatively, a large nappe root is thought to underlie the Greater Caucasus; the top of this root, at the contact of the pre-Jurassic basement and the Jurassic slates and shales would produce a negative impedance contrast. Studies of the structural geology in the Greater Caucasus have indicated that the nappe root may extend to 15 km, the depth of the discontinuity that we have imaged [Dotduyev, 1986]. Furthermore, independent observations of this nappe structure have been observed in the Greater Caucasus by both geologic and geophysical studies [Tagiyev, 1985; Sholpo, 1993].

Near the Dead Sea fault, at station BGIO, we have not found convincing evidence of any crustal thinning. However, we do observe a fairly large variance (± 4 km) for this receiver function

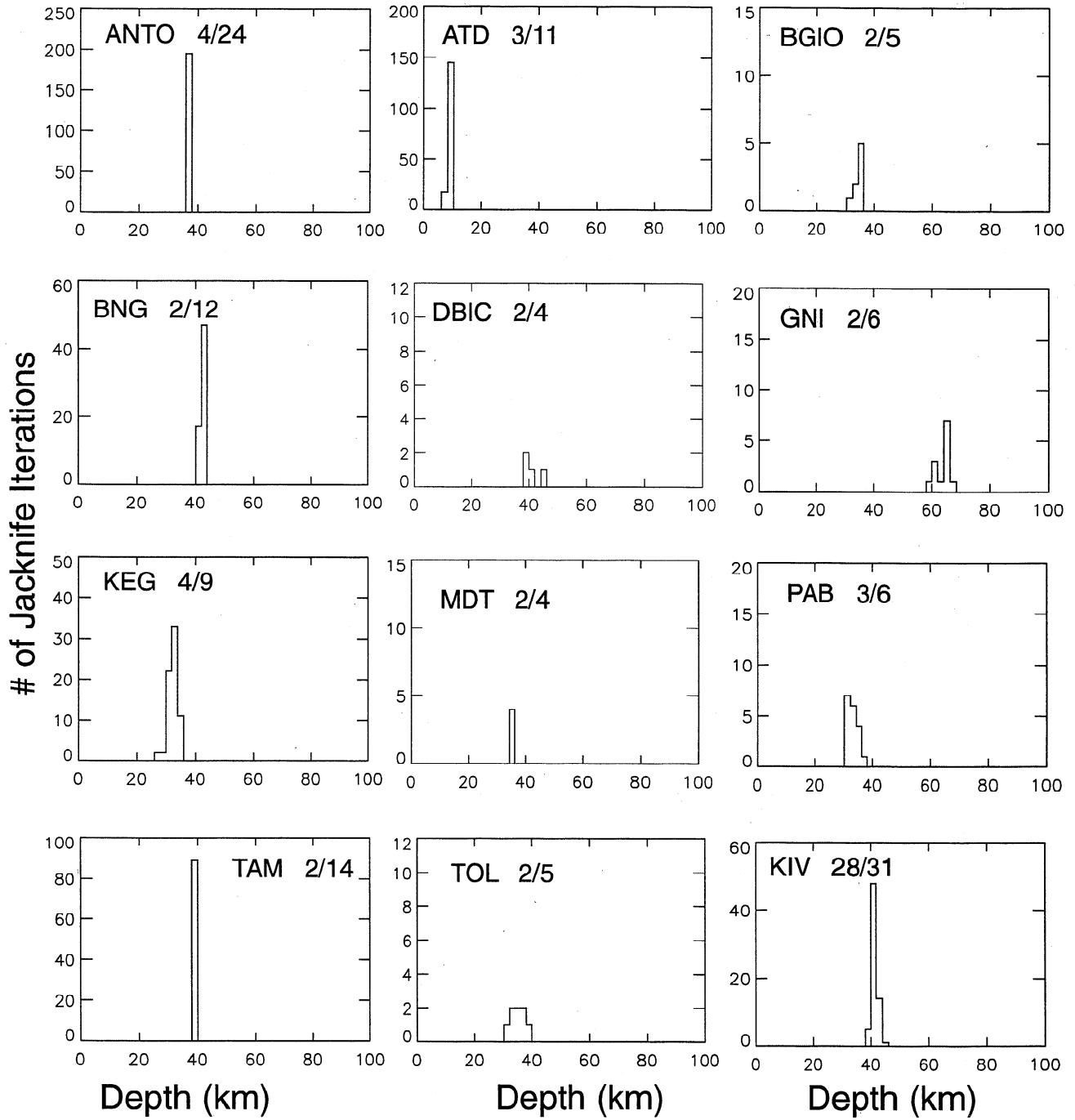


Figure 11. Jackknife histograms of the crustal thicknesses for all 12 stations analyzed in this study. We have determined the number of layers needed to fit the waveforms and then looked at the stability of the depth to the base of the lowest crustal layer using jackknife resampling to obtain each histogram shown. The two numbers to the right of the station name are the number of receiver functions deleted to create each jackknife stack and the total number of receiver functions added into the stack, respectively. Note the large variance in the total number of jackknifed data sets used. This is a function of the number of individual receiver function waveforms available to draw from.

inversion model. The BGIO and KEG shear velocity models are consistent with the refraction models in the region [Ginzburg *et al.*, 1981; Makris *et al.*, 1988; Yuval and Rotstein, 1987]. It is surprising that even our results that are not very stable (i.e., models for stations BGIO and KEG) agree well with other independent estimates of crustal structure. All prior estimates of crustal thickness in this region fall well within our jackknife error estimates, implying that systematic noise does not have a large effect in these stations' inversion results. This is a good

indication that the depth to basement, where it exists, can in many cases be resolved from receiver function inversions. There is a trade-off in resolution with the measurement of basement thickness and measurement of crustal thickness. Receiver functions, with large PS_{basement} phases tend to have distorted and less coherent PS_{Moho} phases.

Our crustal structure measurements in the Middle Atlas, at station MDT, is important confirmation of prior work that has indicated that there is not a significant crustal root beneath the

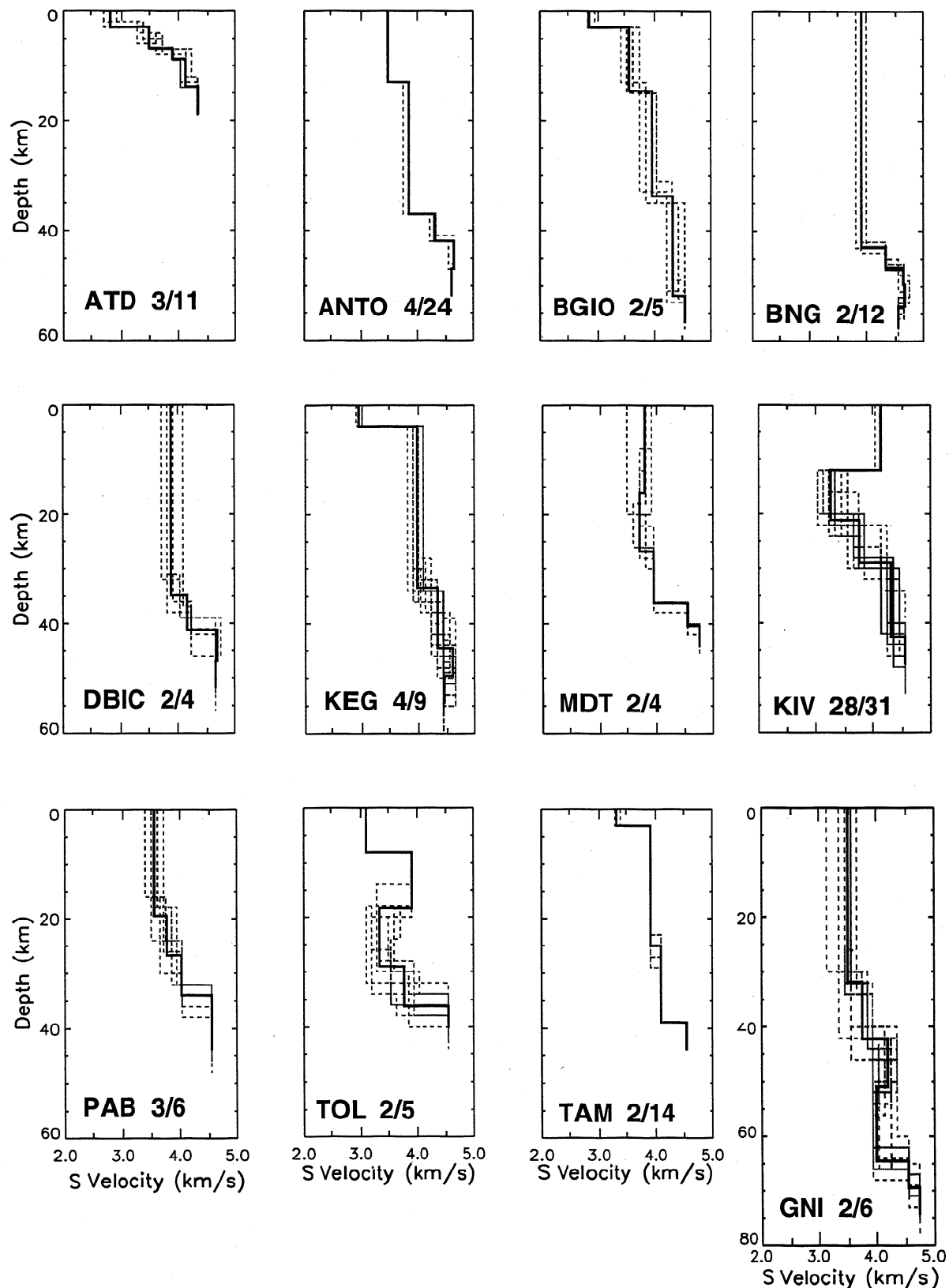


Figure 12. Jackknife shear velocity models for all 12 stations used in this study. These velocity models correspond to models obtained from the resampled receiver function stacks (shown as dashed gray lines). The solid line indicates the mean model. The two numbers to the right of the station name are the number of receiver functions deleted to create each jackknife stack and the total number of receiver functions added into the stack, respectively. The variance of the jackknife shear wave velocity models indicate how stable each receiver function inversion is.

Table 2. Our Best Measurements of Crustal Thickness Using Our Stacked Receiver Functions

Name	Latitude, deg	Longitude, deg	Crustal Thickness, km	Number of Events stacked	Jackknife Iterations
ATD	11.53	42.85	8.0 ± 1.5	11	165
ANTO	39.86	32.79	37.0 ± 1.3	24	90
BGIO	31.72	35.09	33.0 ± 3.3	6	10
BNG	4.44	18.55	43.0 ± 2.1	13	90
DBIC	6.68	-4.86	41.0 ± 4.0	5	6
GNI	40.05	44.72	64.0 ± 4.8	8	15
KEG	29.93	31.83	33.0 ± 4.1	9	84
KIV	43.96	42.69	43.0 ± 5.0	35	90
MDT	32.82	-4.61	36.0 ± 1.3	4	6
PAB	39.55	-4.35	34.0 ± 2.7	9	20
TAM	22.79	5.53	38.0 ± 0.0 (<1.0)	14	91
TOL	39.88	-4.05	34.0 ± 4.1	6	10

The error has been calculated from the variance of the jackknife model parameters. The number of jackknife resampled data sets that are used are also given. Those stations with fewer than 50 jackknife iterations are statistically undersampled; therefore these error estimates are not as reliable.

Middle or High Atlas mountains. Station MDT is in the vicinity of these two mountain ranges, but Wigger *et al.* [1992] profiles cross these two mountain ranges as well as coming to within 10 km of station MDT. The receiver function model agrees very well with the Wigger *et al.* [1992] velocity models beneath the Missour basin, on the flanks of the Middle and High Atlas. Therefore this is circumstantial evidence that Wigger et al.'s image of a flat Moho beneath the Middle Atlas is correct. Beneath station TAM, located near the Hoggar hot spot, we have observed very well constrained crustal thickness measurements that are not significantly thinner than the crustal thickness measurements we have made in the other regions of the African craton (stations BNG and DBIC). This is an indication that the mantle plume beneath TAM has not significantly altered the crustal structure. Stations BNG, DBIC, and TAM are separated by ~500 km, yet receiver function velocity models for these are all fairly similar. Each of these stations has a fairly simple crust, with no evidence of major velocity discontinuities within the crust. These models also all have ~40 km thick crust. This may be an indication that the African craton is fairly uniform in crustal

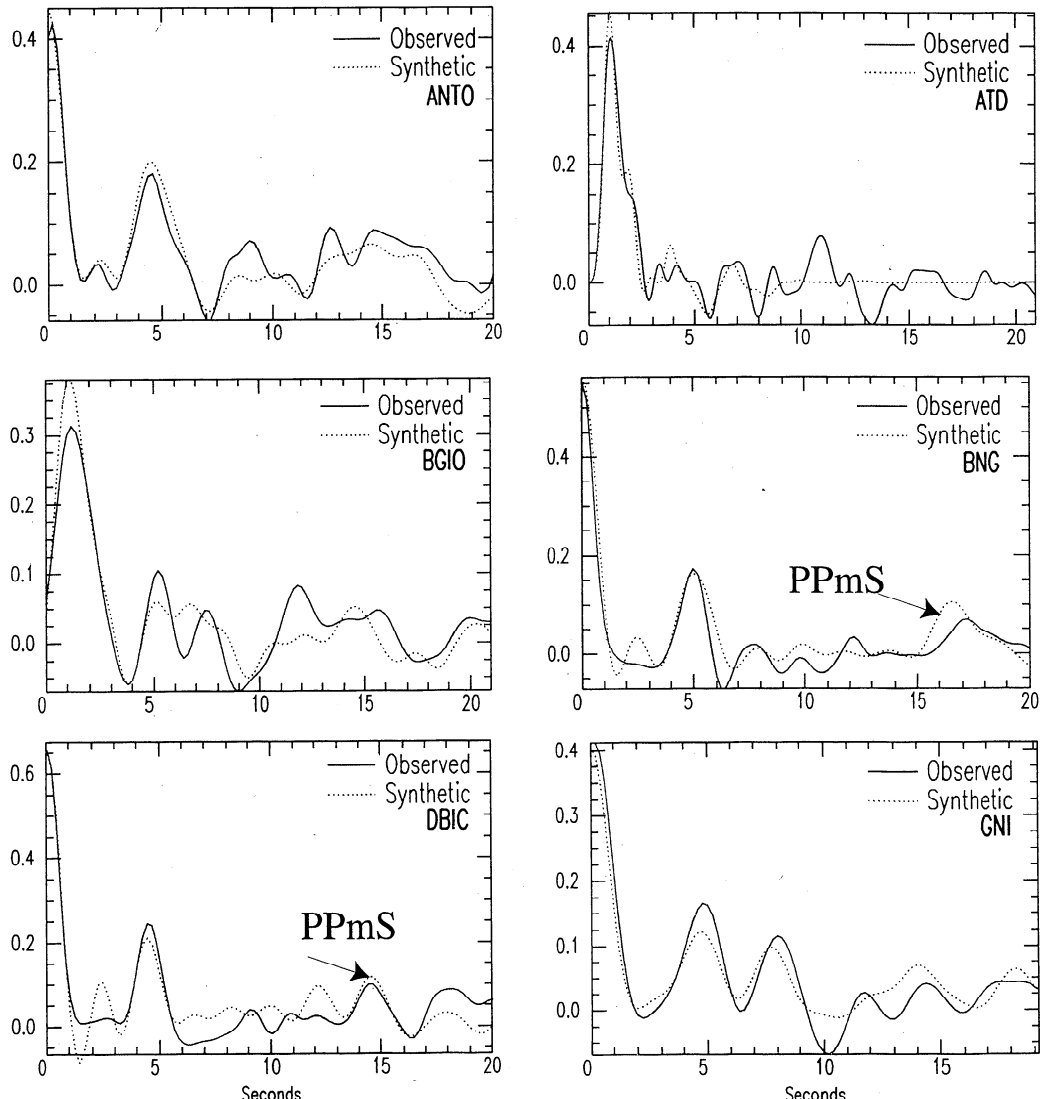


Figure 13. The resulting waveform fits from the 12 receiver function inversions we have performed. The dashed lines are the synthetics, while the solid lines are the observed stacked receiver function waveforms. We are able to obtain relatively good fits between the observed and synthetic receiver functions when using models with four or fewer layers in the grid search inversions.

thickness and structure. However, since we have data for only three stations in the African craton, we cannot make any firm conclusions concerning crustal structure throughout this region.

The grid search scheme presented in this paper is a general and systematic method for determining first-order crustal seismic velocity features from receiver function waveforms. Furthermore, the jackknife error estimation is a new method that, when combined with the grid search scheme, will yield relatively unbiased estimation of waveform inversions stability. Owing to noise sensitivity of most waveform inversions, stability estimation

is essential in determining the reliability of the final models. The jackknife resampling method offers a relatively unbiased and robust estimate of the stability when enough data are available to construct 50 or more jackknifed resampled data sets. Our estimations of variance appear consistent with qualitative observations of data quality and azimuthal variance. When sufficient data are present the jackknife algorithm can be used to estimate uncertainty as a function of azimuth. In summary, we have demonstrated that the grid search inversion method along with the jackknife stability test yield reliable one-dimensional

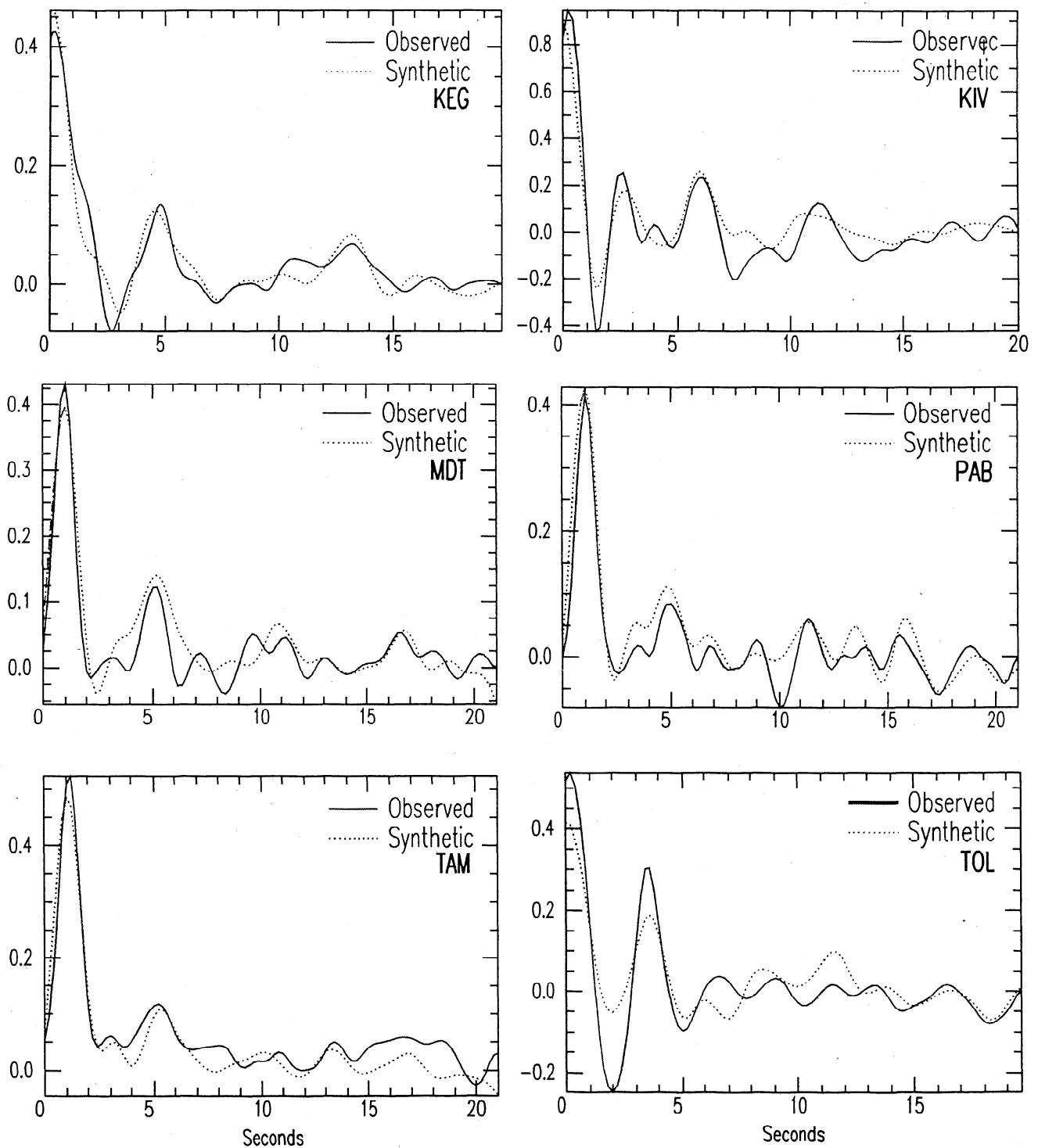


Figure 13. (continued)

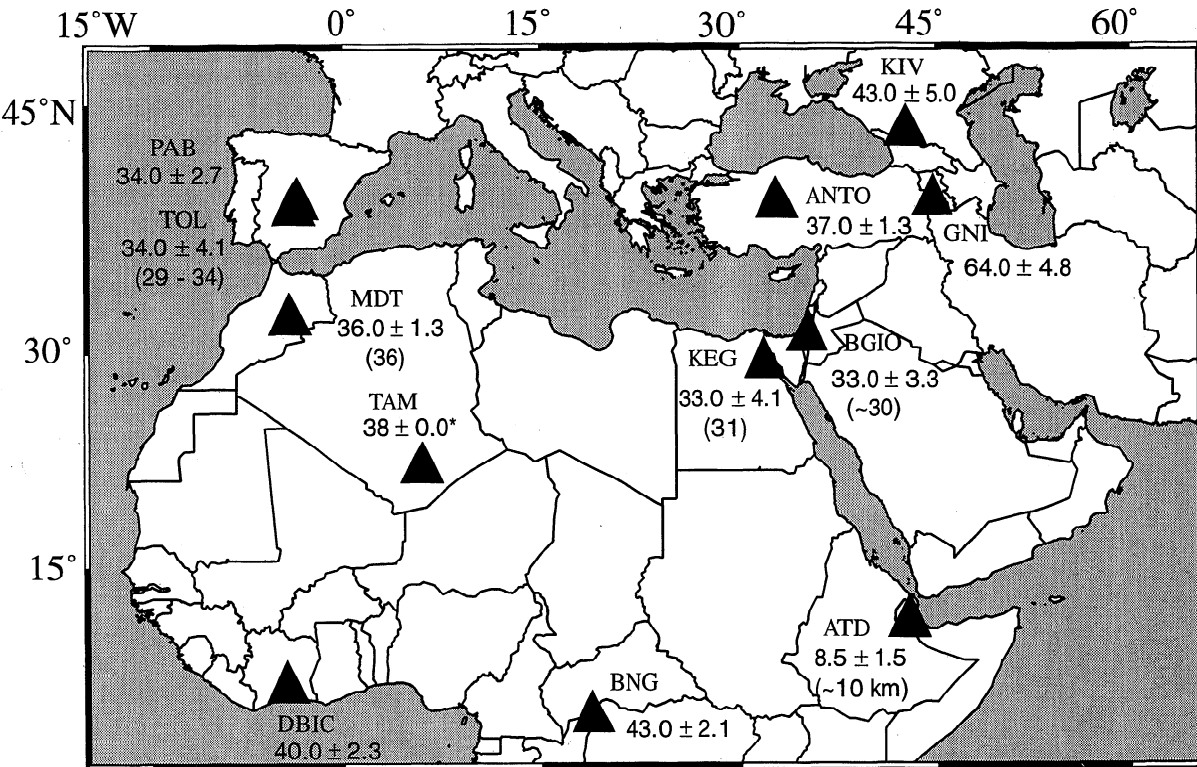


Figure 14. A map showing the grid search results of crustal thickness and prior, if available, estimates of crustal thickness (shown in parentheses), and jackknife error estimates in the Middle East and Africa.

large-scale, first-order crustal structure. The grid search method is the only way to guarantee an optimal and simple solution for the receiver function waveform inversion. We have found significant differences in models obtained from the grid search and the linearized least squares method for station KEG and BGIO. We prefer the grid search technique since it tends toward the minimum length solution and does not introduce a great deal of model complexity that, judging from our error estimates for stations in the Middle East and North Africa, cannot be resolved.

Acknowledgments. We thank the people who run the IRIS, MEDNET, Geoscope, and GEOFON broadband networks for providing us with the high-quality broadband data required for this study. We also thank Tom Hearn (New Mexico State University), Ali Hadi (Cornell University), and Eli Baker (Maxwell Technologies) for very useful discussions on inversion and error estimation procedures. We thank John Cassidy, Arthur Rodgers, and George Zandt for their insightful and helpful reviews. We especially thank Jim Ni (New Mexico State University) for his help and the additional use of his computer resources. This research was mostly sponsored and supported by the U.S. Department of Energy contract F19628-95-C-0092, issued by Phillips Laboratory, and partially supported by the National Science Foundation grant EAR-9627855.

References

- Ammon, C. J., G.E. Randall, and G. Zandt, On the nonuniqueness of receiver function inversion, *J. Geophys. Res.*, 95, 15,303-15,318, 1990.
- Baker, G.E., J.B. Minster, G. Zandt, and H. Gurrola, Constraints on crustal structure and complex Moho topography beneath Pinon Flat, California from teleseismic receiver functions, *Bull. Seismol. Soc. Am.*, 86, 1830-1844, 1996.
- Burdick, L.J., and C.J. Langston, Modeling crustal structure through the use of converted phases in teleseismic body-wave forms, *Bull. Seismol. Soc. Am.*, 67, 677-691, 1977.
- Cassidy, J., Numerical experiments in broadband receiver function analysis, *Bull. Seismol. Soc. Am.*, 82, 1453-1474, 1992.
- Cassidy, J., A comparison of the receiver structure beneath stations of the Canadian National Seismograph Network, *Can. J. Earth Sci.*, 32, 938-951, 1995.
- Cermak, V., and L. Rybach, *Terrestrial Heat Flow and the Lithosphere*, Springer-Verlag, New York, 1987.
- Dotdudev, S.I., The nappe structure of the Great Caucasus (in Russian), *Geotektonika*, 5, 94-105, 1986.
- Efron, B., *The Jackknife, Bootstrap, and Other Resampling Plans*, Soc. of Ind. and Appl. Mech., Philadelphia, Pa., 1982.
- El-Isa, Z.H., J. Mechie, J. Makris, and R. Rihm, A crustal structure study of Jordan derived from seismic refraction data, *Tectonophysics*, 138, 235-253, 1987.
- Gazis, C., M. Lanphere, H. Taylor, and A. Gurbanov, $^{40}\text{Ar}/^{39}\text{Ar}$ and $^{18}\text{O}/^{16}\text{O}$ studies of the Chegem ash-flow caldera and the Eldjurta granite: Cooling of two late Pliocene igneous bodies in the Greater Caucasus Mountains, Russia, *Earth Planet. Sci. Lett.*, 134, 377-391, 1995.
- Ginzburg, A., and Y. Folkman, The crustal structure between the Dead Sea Rift and the Mediterranean Sea, *Earth Planet. Sci. Lett.*, 51, 181-188, 1980.
- Ginzburg, A., J. Makris, K. Fuchs, and C. Prodehl, The structure of the crust and upper mantle in the Dead Sea Rift, *Tectonophysics*, 80, 109-119, 1981.
- Gurrola, H., E. Baker, and B. Minster, Resolution of Receiver Function waveforms and resulting limitations in the modeling of earth structure, *Eos Trans. AGU*, 77, 460, 1996.
- Hofstetter, A., L. Feldman, and Y. Rotstein, Crustal structure of Israel: constraints from teleseismic and gravity data, *Geophys. J. Int.*, 104, 371-379, 1991.
- ILIHA DSS Group, A deep seismic sounding investigation on lithospheric heterogeneity and anisotropy in Iberia, *Tectonophysics*, 221, 35-51, 1993.
- Jenkins, G.M., and D.G. Watts, *Spectral Analysis and Its Applications*, Holden-Day, San Francisco, Calif., 1968.
- Kennett, B., *Seismic Wave Propagation in Stratified Media*, Cambridge Univ. Press, New York, 1984.

- Langston, C.A., The effect of planar dipping structure on source and receiver responses for constant ray parameter, *Bull. Seismol. Soc. Am.*, 67, 1,029-1,050, 1977.
- Langston, C.A., Structure under Mount Rainier, Washington, inferred from teleseismic body waves, *J. Geophys. Res.*, 84, 4749-4762, 1979.
- Laughton, A.S., and C. Tramontini, Recent studies of the crustal structure in the Gulf of Aden, *Tectonophysics*, 8, 359-375, 1969.
- Makris, J., and A. Ginzburg, The Afar depression: Transition between continental rifting and sea-floor spreading, *Tectonophysics*, 141, 199-241, 1987.
- Makris, J., R. Rihm, and A. Allam, Some geophysical aspects of the evolution and the structure of the crust in Egypt, in *The Pan-African Belt of Northeast Africa and the Adjacent Areas*, edited by S. El-Gaby and R.O. Gerling, pp. 345-369, Vieweg, Wiesbaden, Germany, 1988.
- Mohr, P., Nature of the crust under Afar: New igneous, not thinned continental, *Tectonophysics*, 46, 369-406, 1989.
- Owens, T.J., R.S. Crosson, and M.A. Hendrickson, Constraints on the subduction geometry beneath western Washington from broadband teleseismic waveform modeling, *Bull. Seismol. Soc. Am.*, 78, 1219-1234, 1988.
- Paulssen, H., and J. Visser, The crustal structure in Iberia from P wave coda, *Tectonophysics*, 221, 111-123, 1993.
- Phinney, R.A., Structure of the Earth's crust from spectral behavior of long-period body waves, *J. Geophys. Res.*, 69, 2997-3017, 1964.
- Sandvol, E. A., and T. Hearn, Bootstrapping shear wave splitting errors, *Bull. Seismol. Soc. Am.*, 84, 1971-1977, 1994.
- Searle, R.C., The dispersion of surface waves across the Afar, in *Afar Depression of Ethiopia*, edited by A. Pilgerand and A. Roesler, pp. 113-120, Schwizerbart, Stuttgart, Germany, 1975.
- Sheehan, A., G. Abers, C.H. Jones, and A. Lerner-Lam, Crustal thickness variations across the Rocky Mountain front from teleseismic receiver functions, *J. Geophys. Res.*, 100, 20,391-20,404, 1995.
- Sholpo, V.N., Structure of inversion anticlinoria in the core of the Greater Caucasus; An advection hypothesis, *Geotectonics*, 27, 245-251, 1993.
- Silver, P., and W. Chan, Shear wave splitting and mantle deformation, *J. Geophys. Res.*, 96, 16,429-16,454, 1991.
- Surinach, E., and R. Vegas, Lateral inhomogeneities of the Hercynian crust in central Spain, *Phys. Earth Planet. Inter.*, 51, 226-234, 1988.
- Tagiyev, R.E., New data on the structure of the Kura Basin and the southeasterly plunge of the Greater Caucasus, *Geotectonics*, 18, 444-447, 1985.
- Tichelhaar, B., and L. Ruff, How good are our best models? Jackknifing, bootstrapping, and earthquake depth, *Eos, Trans. AGU*, 70, 605-606, 1989.
- Wigger, P., G. Asch, P. Giese, W.D. Heinsohn, S.O. El Alami, and F. Ramdani, Crustal structure along a traverse across the Middle and High Atlas mountains derived from seismic refraction studies, *Geol. Rundsch.*, 81, 237-248, 1992.
- Wu, C.J.F., Jackknife, bootstrap and other resampling methods in regression analysis, *Ann. Stat.*, 14, 1,261-1,295, 1986.
- Yuval, Z., and Y. Rotstein, Deep crustal reflection survey in central Israel, *J. Geodyn.*, 8, 17-31, 1987.
- Zandt, G., and C. Ammon, Continental crust composition constrained by measurements of crustal Poisson's ratio, *Nature*, 374, 152-155, 1995.
- Zhao, L., and C. Frohlich, Teleseismic body-waveforms and receiver structures beneath seismic stations, *Geophys. J. Int.*, 146, 355-370, 1996.
- Zonenshain, L.P., M.I. Kuzmin, and L.M. Natapov, *Geology of the USSR: A Plate Tectonic Synthesis*, *Geodyn. Ser.*, vol. 21, edited by B.M. Page, pp.171-175, AGU Washington D.C., 1990.
-
- M. Barazangi, A. Calvert, E. Sandvol, and D. Seber, Institute for the Study of the Continents, Snee Hall, Cornell University, Ithaca, NY, 14853-1504. (e-mail: sandvol@geology.cornell.edu)

(Received November 12, 1998; revised May 5, 1998;
accepted June 23, 1998)